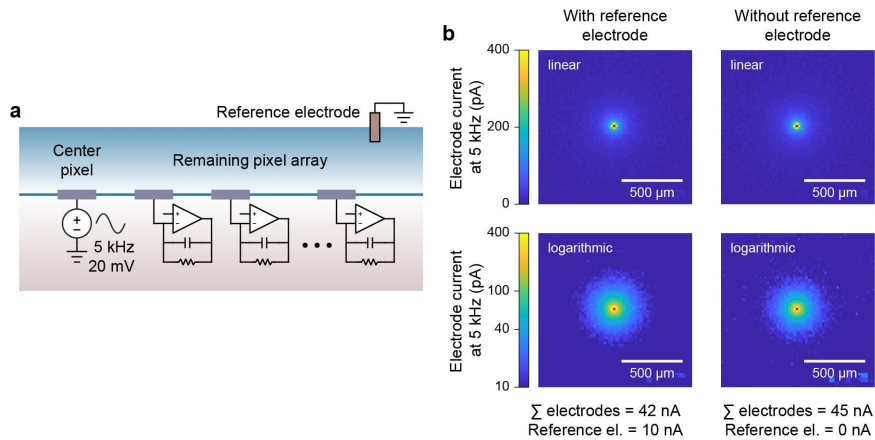
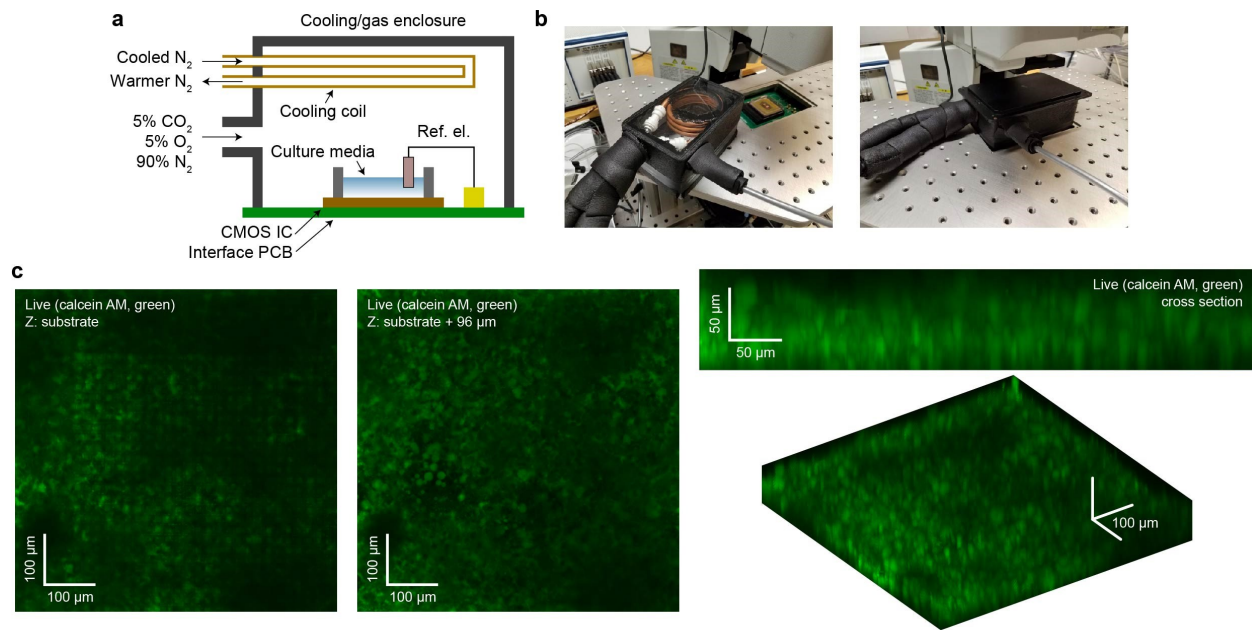


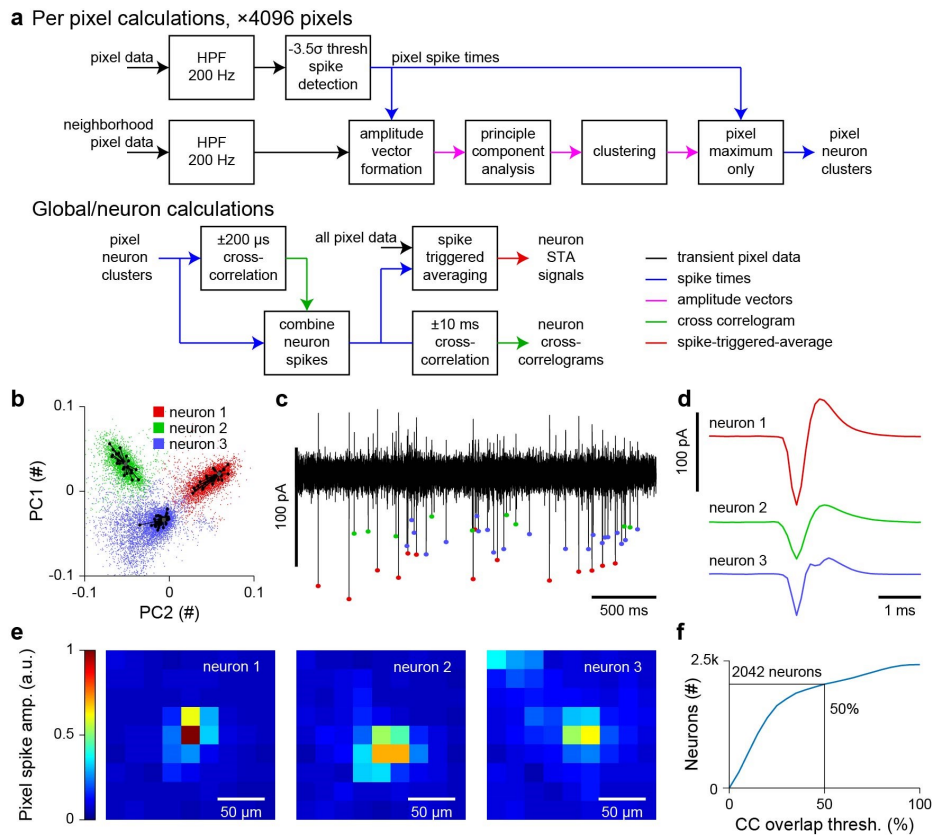
Supplementary Fig. 1 | Additional comparison between voltage amplification and current amplification to supplement Fig. 1c-d. **a**, Simulated gain, V_{amp}/I_{ap} , over frequency for both voltage and current amplification using the schematic of Fig. 1c, the implemented op-amp circuit model, $C_e = 100$ pF, and $R_s = 1$ M Ω . For reference, voltage and current amplification are shown for an ideal op-amp, $R_p = \infty$, and $C_f = 0$. The input referred noise of the current/voltage amplification is calculated as 6.9 pA_{RMS}/ 10.6 pA_{RMS} integrated between 0.1 Hz and 100 kHz, the electrode contributes about 4% of the noise due to its large capacitance reducing its thermal noise, while the remainder is mostly from R_s that is set to 1 M Ω in our calculations and based on our measurements. **b**, The magnitude of EAP voltage amplitudes ($|\Delta V_{ap}|$) and noise threshold of 5 standard deviations (5σ) for 2,041 pixels are shown on the top, bin size 4 μ V. The magnitude of EAP current amplitudes ($|\Delta I_{ap}|$) and noise are shown on the bottom for the same set of pixels recording from the same neurons, bin size 4 pA.



Supplementary Fig. 2 | Measurement of the effects of the reference electrode and electrode array biased with transimpedance amplifiers. **a**, To measure the effects of the reference electrode, a 5 kHz, 20 mV amplitude AC voltage signal was applied to the center pixel while the current through the remaining 4,095 electrodes were measured with transimpedance amplifiers and biased at ground. The Pt reference electrode was also biased at ground with its current being measured using an off-chip transimpedance amplifier. **b**, Heatmap plots of current distribution measured across the array with (left) and without (right) the reference electrode using a linear scale (top) and logarithmic scale (bottom). When in solution, the reference electrode collects 19% of the passed current while the remaining 81% current is collected by the electrode array. Removing the reference electrode decreases the impedance seen by each electrode by only 13%. As such, we observe no difference in extracellular electrophysiological recordings with or without the reference electrode.

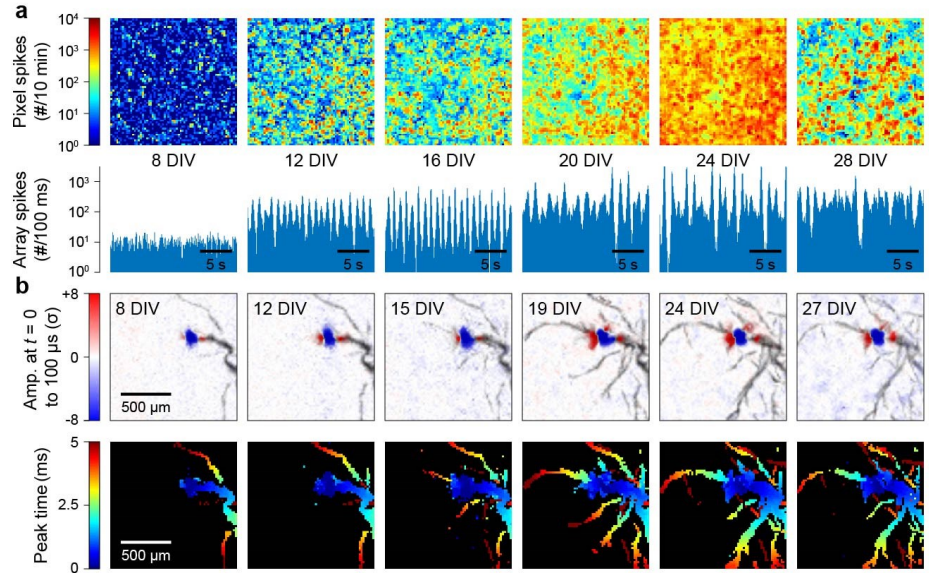


Supplementary Fig. 3 | Measurement setup and imaging of neuron density. **a**, A cooling and gas enclosure is used to improve cell viability during recordings. Due to heat generated from the CMOS circuits, cooled N_2 gas is flowed through a coil inside the chamber to reduce the temperature of the device to $\sim 25^\circ\text{C}$ without any additional device heating. Temperature sensors and heater integrated next to the electrode array are then used to heat the device's surface and neurons on top to the desired temperature for recording, 34°C . **b**, Images of the cooling/gas enclosure; the enclosure is made to be opaque to prevent any light from affecting the CMOS circuits/recordings. **c**, Confocal imaging of a dense dissociated rat neuron culture on top of the CMOS electrode array. The used cultures exhibit multiple cell layers reaching thicknesses of $\sim 100\ \mu\text{m}$.

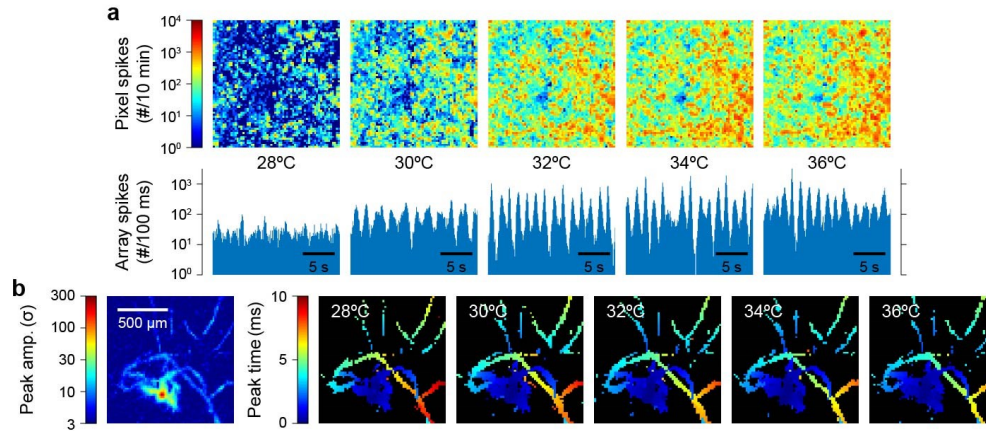


Supplementary Fig. 4 | The implemented spike sorting algorithm. **a**, Flow chart of spike sorting algorithm for a per pixel (top) and global (bottom) basis. Transient data from the origin pixel is first high pass filtered (HPF) at 200 Hz and spike detection at a threshold of -3.5σ is then performed. An amplitude vector is constructed for each spike time using the neighboring pixel data; up to 9×9 pixels centered at the origin pixel. Principle component analysis (PCA) and clustering are then performed using the amplitude vectors. Only neurons wherein the amplitude maximum occurs at the origin pixel are used for further global calculations. The spike times from the resultant neuron clusters from all pixels are used for a cross-correlation ($\pm 200 \mu\text{s}$) to identify any remaining identical neurons. **b**, Example of the first two principle components for three neurons identified from an example pixel recording. **c**, The transient data from the example pixel with each neuron spike identified after clustering. **d**, Average spike waveforms for each of the three neurons. **e**, Identified amplitude vectors for each neuron; only neuron 1 would be used for

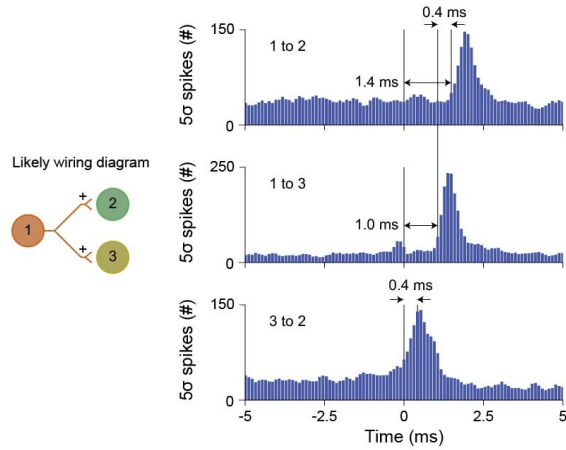
global calculations as it is the only neuron with a maximum at the origin pixel. e, Elimination of identical neurons using cross correlation for a given spike time overlap percentage. This step eliminates neurons being measured at similar maximum amplitudes at more than one pixel (e.g. neuron 2): 2,042 unique neurons are identified at a 50% cross-correlogram overlap percentage threshold.



Supplementary Fig. 5 | Spontaneous neuronal activity and action potential propagation across days *in vitro*. **a**, The activity of a rat neuron culture increases over culture days *in vitro* (DIV) and peaks at 24 DIV; the spikes measured per pixel is shown on the top and the total array spikes across time on the bottom for measurements from 8 DIV to 28 DIV, bin size 100 ms. **b**, An example mapping of a neuron throughout the duration of the culture. An overlay (top) of the signal polarity (red/blue) during the EAP (average of $t = 0 \mu\text{s}$ to $100 \mu\text{s}$) and the neurons electrical imprint (black/grey) shows both dendritic (red) and axon tree growth (grey). The signal propagation velocity is seen to decrease significantly over time (bottom); see also Supplementary Video 5 [$n = 2,400$ for each of the averages].

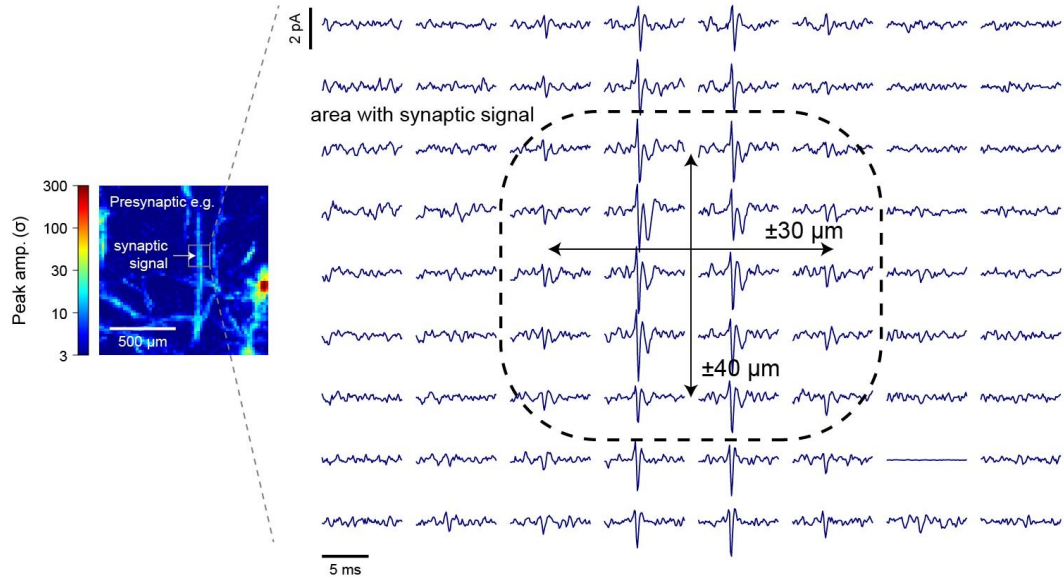


Supplementary Fig. 6 | Spontaneous neuronal activity and action potential propagation across temperature. **a**, The activity of the culture was observed to increase with temperature, measured at 20 DIV; measurements were performed at 28-36°C, bin size 100 ms. **b**, The mapping of a neuron (left) and its propagation (right) shows a significant increase in propagation velocity with increasing temperature; see also Supplementary Video 6. All other recordings are performed at 34°C.

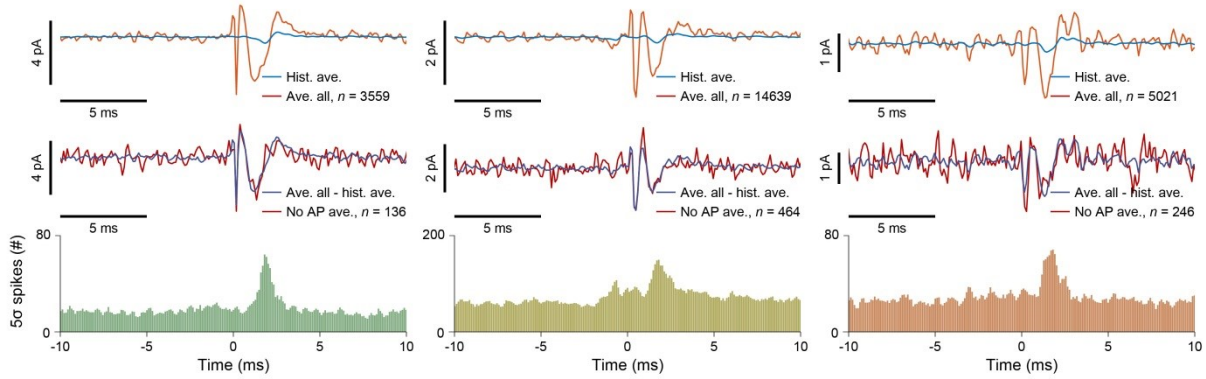


Supplementary Fig. 7 | Example of ambiguous cross-correlograms for synaptic mapping.

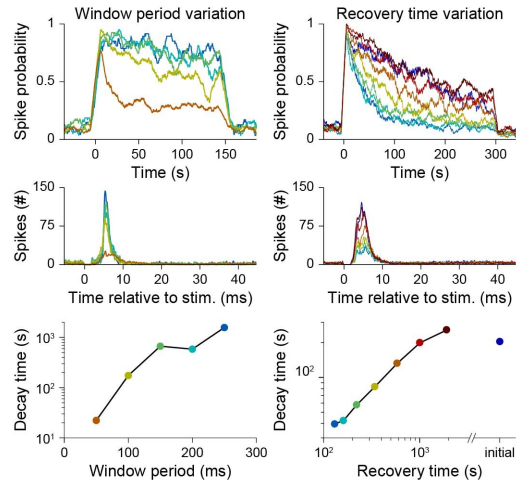
The likely wiring diagram (left) of three neurons (neurons 1, 2, and 3) and their corresponding cross-correlograms (right). The difference in propagation delay from 1 to 2 (1.4 ms) and 1 to 3 (1.0 ms) results in a correlogram that looks like a synaptic connection between 3 to 2 with a delay corresponding to the time difference (0.4 ms).



Supplementary Fig. 8 | Spatial profile of a synaptic signal along an axon. A synaptic signal is observed in a neuron's STA (left) with a clear spatial profile (right). The synaptic signal is measured across a region of 5×4 group of pixels indicating a spatial spread similar to that of the axon.



Supplementary Fig. 9 | Additional data for extracellular synaptic signal. To investigate the effects of post-synaptic APs on the average extracellular synaptic signal, STA was performed for all pre-synaptic detected spikes (ave. all, top) and for pre-synaptic spikes without a detected post-synaptic AP (no AP ave., middle), as determined as a post-synaptic range less than 2σ for ± 15 ms around the pre-synaptic spike time. For comparison, the average post-synaptic AP signal was used in conjunction with the cross-correlogram (bottom) to generate the effective contribution of APs on the average extracellular signal (hist. ave., top). Subtraction of this signal from the STA average signal (ave. all - hist. ave, middle) closely resembles the no AP average signal. The subtracted signal is plotted in Fig. 2 due to its higher signal to noise ratio.



Supplementary Fig. 10 | Window period and recovery time variation. The declining probability over time (top) and spike histogram (middle) are affected by the window period and recovery time (the window period histograms have been normalized to the 50 ms window due to the difference in total windows). An exponential decay is fit to the probability over time to define a decay time constant (bottom); note the logarithmic y-axis. The results support a declining probability due to synaptic fatigue and a broadened histogram due to post-synaptic potential summation jitter.